Science Translational Medicine
AAAS

stm.sciencemag.org/cgi/content/full/12/526/eaay1769/DC1

Supplementary Materials for

Cerebellar oscillations driven by synaptic pruning deficits of cerebellar climbing fibers contribute to tremor pathophysiology

Ming-Kai Pan*, Yong-Shi Li, Shi-Bing Wong, Chun-Lun Ni, Yi-Mei Wang, Wen-Chuan Liu, Liang-Yin Lu, Jye-Chang Lee, Etty P. Cortes, Jean-Paul G. Vonsattel, Qian Sun, Elan D. Louis, Phyllis L. Faust, Sheng-Han Kuo*

*Corresponding author. Email: emorymkpan@ntu.edu.tw (M.-K.P.); sk3295@columbia.edu (S.-H.K.)

Published 15 January 2020, *Sci. Transl. Med.* **12**, eaay1769 (2020)
DOI: 10.1126/scitranslmed.aay1769

The PDF file includes:

Other Supplementary Material for this manuscript includes the following:

(available at stm.sciencemag.org/cgi/content/full/12/526/eaay1769/DC1)

Movie S1 (.mp4 format). Tremor characteristics in WT versus *Grid2*^{dupE3} mice.
Movie S2 (.mp4 format). Tremor modulation by dry ice–mediated cerebellar lesioning.
Movie S3 (.mp4 format). Tremor modulation by optogenetic inhibition of cerebellar outputs.
Movie S4 (.mp4 format). Tremor modulation by synaptic inhibition of CFs.
Movie S5 (.mp4 format). Tremor induction by PC stimulation in a WT mouse.
Data file S1. Raw data (provided as separate excel file).

SUPPLEMENTARY MATERIALS AND METHODS

Selection of postmortem human brains.

Subject selection was determined by the available postmortem control cerebellum for the current study. We first identified 15 controls above age of 70 from the New York Brain Bank with available formalin-fixed tissues, and we selected 19 patients with ET to age-match with these controls for the immunohistochemistry analysis. We chose 15 patients with ET and 15 age-matched controls for the Western blot analysis based on the availability of the frozen cerebellar tissues. Among the selected cases and controls, there were 11 patients with ET and 8 controls with both formalin-fixed and frozen tissues for the correlation analysis.

We excluded cases with ET but also brainstem Lewy body pathology (*64*) or pathology of progressive supranuclear palsy. The clinical diagnosis of ET was first made by the treating neurologists, and subsequently confirmed by an Essential Tremor Centralized Brain Repository movement disorders neurologist (EDL) using clinical questionnaires, medical records, videotaped neurological examination, and assessment of standardized Archimedes spirals. Each ET case had a standardized, videotaped neurological examination to evaluate tremor characteristics and tremor severity in detail. The severity of tremor was determined using the total tremor score [TTS] (range 0-36), based on the ratings of tremor on videotaped examination, which generally occurred within six months of death.

The control brains were from individuals who participated in the Alzheimer's Disease Research Center and the Washington Heights Inwood Columbia Aging Project at Columbia University. These individuals were followed prospectively with serial neurological examinations and were free of Alzheimer's disease, ET, PD, Lewy body dementia, or progressive supranuclear palsy in the clinical examination during life. All subjects signed informed consent of the Institutional Review Board of respective institutions (Columbia and Yale Universities).

All brains received standardized assessment of Lewy body pathology and tau and beta-amyloid immunohistochemistry as previously described (*64*). We chose to study the anterior lobes of the cerebellar cortex, which is responsible for the motor function. We obtained paraffin sections (7μm thick) or frozen tissues from this region of the cerebellum to perform immunohistochemistry and Western blot analysis, respectively.

Selection of participants for the EEG study.

Patients with ET were recruited from the Center for Parkinson's Disease and Other Movement Disorders at Columbia University or the Movement Disorders Clinic at National Taiwan University Hospital, and also from flyers sent out by the International Essential Tremor Foundation. Controls were recruited from patients' friends or spouses and were examined to be free of tremor. All subjects were examined by a movement disorders specialist (SHK or MKP) to confirm the diagnosis of ET, and patients with ET were free of parkinsonism or dystonic features. All the participants signed informed

consent approved by the Institutional Review Board of Columbia University or National Taiwan University Hospital.

Animals

We studied adult *hotfoot17J* mice (Jackson Laboratory, No. 005718) with dramatically reduced GluRδ2 levels (GluRδ2 insufficiency) as the mouse model of tremor and PC synaptic pathology. WT littermates were used as experimental controls. Both male and female mice showed similar tremor and motor coordination profiles in both genders were included in this study. The mouse genotypes were confirmed by RT-PCR of the cerebellar cortex (see method below). We also studied *hotfoot4J* mice (Jackson Laboratory No. 000548), another mouse line with GluRδ2 deficiency (*25*) to confirm the observation in *hotfoot17J* mice. Mice were housed in the central and satellite facilities of Columbia University Medical Center and National Taiwan University with controlled dark-light cycle. All procedures were approved by the Institutional Animal Care and Use Committee (IACUC) of Columbia University and National Taiwan University College of Medicine.

Immunohistochemistry for human and mouse cerebellum

Seven μm thick sections of paraffin-embedded human postmortem (paravermis region, 1cm from the midline of the lobule IV-VI) or mouse cerebellar tissues were rehydrated and treated with 3% hydrogen peroxide and antigen retrieval with 0.1M Tris-based urea solution pH 9.5 for 20 minutes (human postmortem cerebellum) or with 0.01M sodium citrate buffer pH 6.0 for 60 minutes (mouse cerebellum), 100^0C. The following primary antibodies were used: VGlut2 (human cerebellum 1:250 (*16*), mouse cerebellum 1:500 SYSY #135404), calbindin (human cerebellum 1:1,000, Sigma c9848; mouse cerebellum 1:200, Santa Cruz sc-7691), GluRδ2 (human cerebellum 1:250, Frontier Institute AF-500; mouse cerebellum: 1:400, Abcam ab190358; 1:50, Santa Cruz sc-39347, 1:500, Swant CB-38), GRP78 (mouse cerebellum: 1:250, Abcam ab21685), GFP (mouse cerebellum 1:500, Aves, GFP-1020), RFP (mouse cerebellum 1:500, Rockland #600-401-379), synaptophysin (1:50, Santa Cruz sc-55570). The sections were incubated with the primary antibodies 24 - 48 hours at 4^0C followed by the secondary antibodies either conjugated with fluorophores or peroxidase, which were developed by 3,3-diaminobenzidine (DAB) precipitation. Bright field images were acquired with the Leica DM6 and fluorescent images were acquired with the Leica TSC SP2 confocal microscopy. CF-PC synapses were visualized with VGluT2 immunohistochemistry whereas PC dendrites were visualized with calbindin immunohistochemistry. We studied CF synapses in the parallel fiber territory of the PC dendrites by quantifying the percentage of CFs extending to the outer 20% of the molecular layer, as previously described (*15, 16*).

Western blot analysis

Frozen postmortem human or fresh mouse cerebellar cortex were solubilized in RIPA buffer supplemented with proteinase inhibitors and phosphatase inhibitors (Roche Diagnostics). Tissues were sonicated briefly and centrifuged. Protein concentrations were determined by PierceTM BCA Protein Assay Kit (Thermo Scientific). For the postmortem human samples, equal amount of proteins was loaded in the 10% SDS-PAGE. For mouse samples, 4-12% NuPAGE Novex gels (Invitrogen) were used. Proteins were then transferred to a PVDF membrane (Millipore) and blots were incubated with the following primary antibodies: GluRδ2 (1:1,000 BD Transduction Laboratory 611006; 1:1000 Abcam ab198499), β-actin (1:10,000, Santa Cruz sc-47778), mGluR1 (1:500, Abcam ab82211), GAPDH (1:5000, Invitrogen MA5-15738). The blots were further incubated with respective secondary antibodies conjugated with either peroxidase (all 1:10,000 Jackson ImmunoResearch Laboratories) or with respective secondary antibodies conjugated with IRDye® (all 1:10,000 LI-COR). Signals were detected with ECL (Millipore) and BioMax MR film (Sigma) or with Odyssey® CLx Imaging System (LI-COR).

We tested the GluRδ2 protein degradation in live mouse brain slices, and this method was previously used to study synaptic protein degradation. Briefly, four-week-old *hotfoot17J* mice and WT littermates were anesthetized with isoflurane and decapitated. The brains were quickly removed and placed in ice-cold NMDG-HEPES ASCF containing the following (in mM): 92 NMDG, 2.5 KCl, 1.25 NaH_2PO_4, 30 $NaHCO_3$, 20 HEPES, 25 glucose, 2 thiourea, 5 Na-ascorbate, 3 Na-pyruvate, 0.5 $CaCl_2 \bullet 7H_2O$, with the pH at 7.4 by gassing with 95%O_2/ 5% CO_2. The cerebellum was sagittally sliced into 350 μm sections with a tissue slicer (Leica VT1000S; Wetzlar, Germany) and transferred to an interface-type holding chamber with oxygenated ACSF containing the following (in mM): 125 NaCl, 2.5 KCl, 26 $NaHCO_3$, 2.4 $CaCl_2$, 1.3 $MgSO_4$, 0.3 KH_2PO_4, and 10 glucose with either DMSO or 0.1 mM MG-132, or 0.1 mM NH_4Cl_2 with 0.1 mM leupeptin, with the pH maintained at 7.4 by gassing with 95% O_2 and 5% CO_2 at room temperature (25°C). After 6 hours incubation, cerebellar slices were frozen and prepared for Western blot analysis.

RT-PCR

Cerebellar tissues from either WT or *hotfoot17J* mice were homogenized in TRIzol® Reagent (Ambion), and RNA preparation was done by Direct-zolTM RNA miniPrep Plus Kit (Zymo Research). cDNA synthesis was performed by SuperScript® III First-Strand Synthesis SuperMix (Invitrogen) using total RNA primed with random primers. Different exons of GluRδ2 cDNA were amplified by Platinum® Pfx DNA Polymerase (Invitrogen) with primers. We ran the PCR products on agarose gels to compare the size of amplified fragments. We sent purified fragments for the sequence analysis (Genewiz®). The full-length sequences of GluRδ2 cDNA and amino acids from either WT or homozygous *hotfoot17J* mice were aligned by the GeneDoc software.

Tremor recordings in freely moving mice

We applied a platform (Convuls-1, Columbus Instruments) for weight-based vibration detection with linear weight-voltage transformation (141 millivolt per 32 gram of mass per gravity, or 0.45 Volt per Newton). We placed mice on the platform for tremor measurement, which was co-registered with a video-based motion detection (NeuroMotive, BlackRock microsystem) to separate kinetic vs. rest tremor. The videos were taken with the speed of 50 frame-per-second (fps), with the build-in NeuroMotive software to detect the center-of-mass of the mouse, delineated by the black (mouse)-white (background) contrast. Coordinate changes > 0.5 cm between the center-of-mass in the current frame and the frame 1 second ago were coded as movement.The vibratory signals were filtered (low pass filter: 250 Hz) and digitized at 1,000 Hz with DAQ device (Cerebus, BlackRock microsystem). Tremor recordings were performed in mice at the age of 3 months or older except for the study of the age of tremor onset and progression. We performed spectrum analysis for the tremor frequency. Digitized data were processed offline using in-house MATLAB scripts developed for frequency analysis (*65, 66*). Behavioral data were transformed into frequency domains via the power spectrum density function (by Welch's method with Hanning windowing, sampling rate at 1,024 Hz in data block of 1 seconds, given the frequency resolution of 1 Hz and half of the data overlap in each step). Each power spectrum density data point was constructed from a 20-second window and one-second shift for the next data point until the end of data stream. The spectrum data were further normalized to the overall power between 5-55 Hz to eliminate the effect of 60 Hz noises and the variability of absolute power between mice. Data analyses of all mice were performed by these preset programs automatically and blinded to genotyping results. We tested the tremor responsiveness to medications for patients with ET in the mouse model by intraperitoneal administration of primidone (50mg/kg), propranolol (10mg/kg) or ethanol (1.25g/kg) at the doses tested for harmaline and $GABA_A$ receptor knockout rodent tremor models.

Viral-mediated GluRδ2 rescue

For viral-mediated GluRδ2 expression in the cerebellum *in vivo*, we used *Grid2*^{dupE3} mice in their adulthood (> 6 weeks). GluRδ2-GFP Sindbis viral construct was injected into *Grid2*^{dupE3} mice. GluRδ2-GFP Sindbis viral construct was generously provided by Dr. Michisuke Yuzaki (*67*) and was packaged at Sanford Burnham Prebys Medical Discovery Institute at La Jolla, CA. Mice were anesthetized by isoflurane prior to head-fixation on the stereotaxic frame (David Kopf Instruments). Subcutaneous bupivacaine was administered for local anesthesia. The scalp was incised above the cerebellar region after fur removal. Adequate sterilization was applied and the mouse skull was drilled and a 32GA Hamilton syringe containing of Sindbis virus was inserted into the mouse cerebellum at the following coordinates (to Bregma AP: -6.4mm, ML: 0mm, DV: -0.15mm). 5 uL of virus at the rate of 0.66 uL per minute were injected into the subarachnoid space around the mouse cerebellum. Ten minutes after completing injection, syringe was removed at the rate of 0.05 mm per minute. The scalp

was sutured and mice received standard post-operative care. Sindbis viral-mediated expression only took a few days (*24*). The effects of GluRδ2 rescue were confirmed by Western blot analysis. Mouse behavior was tested by tremor analysis using the above mentioned protocol.

Dry ice cerebellectomy.

Each mouse was mounted on the stereotaxic frame with mild anesthesia by isoflurane (respiratory rates ~ 2/sec). After exposing the skull at the cerebellar region, dry ice was shaped to cover 4 mm^2 surface area after lambda fissure, and placed on the skull for 30 seconds with full contact. The wound was sealed with instant glue and the mouse usually recovered within 1 minute. Freely moving behaviors were recorded at baseline and 5-minute after recovery from dry ice cerebellectomy.

Optogenetic inhibition of PC outputs.

Surgical procedures were performed in 3-month old adult *Grid2*^{dupE3} mice and WT littermates. We injected AAV virus carrying CaMKIIa-eNpHR 3.0-EYFP (Virus Vector Core, UNC) in the cerebellar cortex at 8 points (AP, -6.0 & -6.6 mm; ML, ±1.0 mm; DV, -0.3 & -1.3 mm from dura), 0.5 μL of virus in each point with an injection speed of 0.1 μL/min. Fiber optic cannulae (Thorlabs) were implanted into bilateral DCN (AP, -6.24 mm; ML, ± 2.1mm; DV, -1.9 mm from dura) within the same surgical procedure. Initial behavioral experiments started 2 weeks after the surgical procedure. 4 mW of green light (561 nm, OEM laser) was applied via optic fibers attached to the cannulae, and illuminated for 5 minutes in the middle of the 15-minute tremor recording in the freely moving mice (**Fig. 4H**). Non-activating blue light (473 nm, OEM laser) was also applied with the same protocol and served as control experiments. After completed behavioral experiments, mice were perfused with 4% paraformaldehyde for histological validation of cannulae locations and viral expression (**Fig. 4G**).

Optogenetic inhibition of synaptic vesicle release.

We injected AAV virus carrying SYP-miniSOG-citrine (Viral Vector Core, Duke University) into 3-month old adult *Grid2*^{dupE3} mouse IO at 4 points (AP, -7.0 and -7.4 mm; ML, ±0.3 mm; DV, -6.1 mm from bregma), 0.5 μL of virus in each point with injection speed of 0.1 μL/min (**Fig. 5B),** followed by a cranial window above the cerebellum covered by a transparent coverslip (round shape, 3 mm in diameter, Warner Instruments LLC) (**Fig. 5D**). This viral injection was included in all following procedures described in this section. Experiments were performed 2 weeks or later after viral injection. After measuring the baseline tremor, we mounted the mouse onto the stereotaxic frame with mild sedation with isoflurane (0.6~0.8% with flow rate 200 ml/min) and maintaining the breathing rates around 2 Hz. 8 mW of blue light (473 nm) was applied at 0.2 mm above the coverslip, and scanned at 7 points evenly distributed over the coverslip (**Fig. 5D** and **Movie S4**), with each point illuminated for 4 minutes. The mouse usually regained normal grooming behaviors and motility within 30 seconds. Five-minute recordings of tremor were performed at baseline, 0.5, 1, 1.5, 2, and 24 hours after completing blue-light

scanning. We also applied non-activating green light (561 nm) with the same protocol and the same energy to exclude the procedure-related or thermal energy-related effects. We also performed synaptic silencing of olivonuclear fibers. AAV viruses carrying SYP-miniSOG-citrine were injected in bilateral IOs of adult *Grid2*^{dupE3} mice, and fiber optic cannulae were implanted into bilateral DCNs in the same surgical procedure (**Fig. 5I**). In behavioral recordings, optic fibers were connected to the cannulae and transduced up to 8 mW of blue light for 5 minutes. Five-minute recordings of tremor were performed at baseline, 0.5, 1, 1.5, 2, and 24 hours after illumination.

Optical stimulations of PC outputs.

Surgical procedures for viral injection and implantation of fiber optic cannulae were the same for optogenetic inhibition of PC outputs, except that we applied WT mice of 3-month old and injected AAV8 virus carrying CaMKIIa-hChR2-(E123T/T159C)-mCherry (Viral Vector Core, UNC). Initial behavioral experiments started 3 weeks after the surgical procedure. The hChR2 was activated by blue light (473 nm, 4 mW, OEM laser) via optic fibers attached to the cannulae. Illumination was applied as a train of square wave (20 Hz, with 50% of duty cycle) for 2 minutes in the middle of 15-minute tremor recordings in the freely moving mice. Non-activating green light (561 nm, OEM laser) was also applied with the same protocol as the control experiment.

Pharmacological silencing of IO neurons.

Drug infusion cannula (Plastics One) was implanted at coordinates 0.2 mm above IO (AP, -7.4 mm; ML, -0.15 mm; DV, 5.8 mm) in *Grid2*^{dupE3} mice and WT littermates at the age of 3 months or older (**Fig. 4, K to O**) in the following procedures described in this section. *Unit recordings of IO neurons.* A tungsten electrode (diameter 0.002 inch, California Fine Wire Company) was inserted into the IO and recorded multi-unit activities from neurons in situ. An infusion needle (Plastic One) was placed into the cannula and 0.25 mm protruded from the cannula tip. After 5-10 minutes of baseline recordings, 1 μL of 2% lidocaine was infused with the speed of 0.2 μL/min for 5 minutes. Multi-units were recorded continuously for 40-60 minutes with simultaneous cerebral LFP recordings and tremor measurement.

Simultaneous recordings of cerebellar LFPs and tremor in mice

Cerebellar surface electrodes (California Fine Wire Company) were implanted in the mouse cerebellum for chronic LFP recordings in the freely moving mice. Each mouse was anesthetized with isoflurane and mounted on the stereotaxic frame with the skull exposed. Recording electrodes were placed on bilateral cerebellar surface with the following coordinates relative to bregma: AP, -6.4 mm; ML, ±2.0 mm; DV, -0.3 mm (from dura). Reference and ground electrodes were placed in the right and left nasal bone, respectively. Implanted electrodes were fixed on the skull with C&B-METABOND (Personal Dental). Mice were allowed to recovery from surgery for 7 days before the initial recordings. LFP signals were

filtered and digitalized using the same parameters as behavioral signals described above, and simultaneously registered in the same DAQ device for the offline analysis.

Spectrum analysis of tremor and LFP data.

Digitized data were processed offline using in house MATLAB scripts developed for frequency analysis (*65, 66*). Behavioral and LFP data were transformed into frequency domains via PSD function (PSD by Welch's method with Hanning windowing, sampling rate at 1,024 Hz in data block of 1 seconds, given the frequency resolution of 1 Hz and half of the data overlap in each step). Each PSD data point was constructed from a 20-second window and one-second shift for the next data point until the end of data stream. The spectrum data were further normalized to the overall power between 5-55 Hz, to eliminate the effect of 60 Hz noises and variability of absolute power between mice. We also applied coherence analysis (*65, 66*) to evaluate the synchronization between LFP and tremor signals. The coherence data were constructed with the same windowing, overlapping and time-shifting methodology as PSD. Data analysis of all mice were performed by these preset programs automatically and blinded to genotyping results.

Spike-phase coupling

Spike-phase coupling were performed between single-unit spikes from IO and cerebellar LFPs or tremor. Single-unit activity in IO, cerebellar LFPs and corresponding mouse behaviors were recorded as previously described, but sampled in 30,000 Hz. The LFPs or tremor signals were band-pass filtered in 15~25 Hz, in order to focus on the tremor-related phase profiles. Filtered signals underwent Hilbert transformation and phase correction by $\pi/2$. Timestamps of IO spikes were used to extract the corresponding phase in the LFPs or tremor. To quantify the correlation between spikes and phases, we applied polarity index, which is the summation of all phases as unit vectors (vectors with the length equal 1) divided by the number of vectors. Polarity index is a value between 0 and 1, whereas 0 indicates totally random phases and 1 indicates all spikes are landed in the same phase.

EEG recordings and analysis.

Study participants were placed in a 32-channel EEG machine (Cervello 32, BlackRock Microsystem Inc.) with 18 electrodes covering the cerebellar region below the inion (**Fig. 7A**). We recorded EEG signals at rest or during hand movements, which induces tremor in patients with ET. For source localization purpose, we performed 28-channel EEG with standard 10-20 system, with 6 channels at and below the level of inion (**Fig. 7, E and F**). EEG signals were band-pass filtered between 0.3~256 Hz, and digitized at 1,024 Hz. EEG data were analyzed offline with an open source software, Brainstorm (http://neuroimage.usc.edu/brainstorm) for source localization and MATLAB (MathWorks) for further processing of cerebellar EEG signals. In the cerebellar leads, we selected the bipolar EEG montages using an EEG lead located at the cerebellar hemisphere ipsilateral to the dominant hand and

another EEG lead located at the cerebellar vermis contralateral to the dominant hand to broadly sample the signals across the cerebellum. EEG signals were transformed into frequency domain using the same PSD function for mouse LFP analysis, and also the same windowing, overlapping and time-shifting methodology except that each data point was constructed from a 10-second window.

SUPPLEMENTARY FIGURES

Supplementary Figure 1

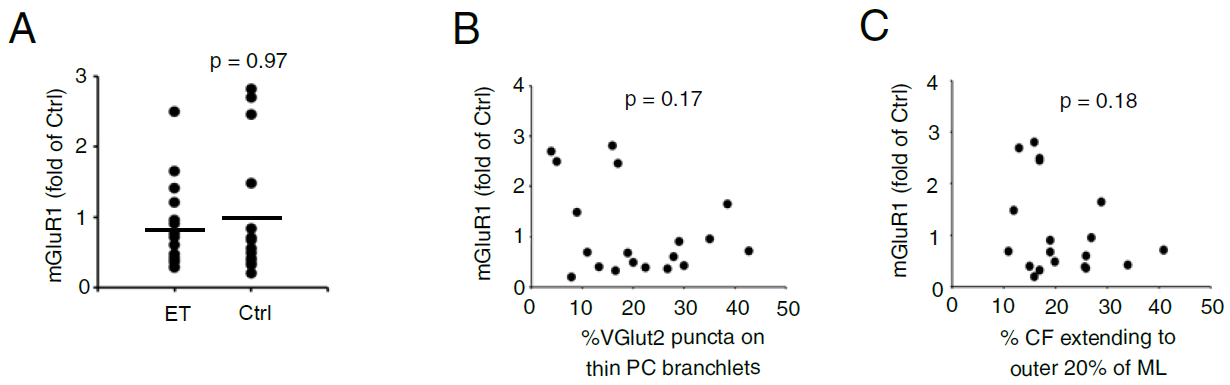

Fig. S1. mGluR1 expression in the postmortem ET cerebellum. (**A**) Quantification of mGluR1 expression of the postmortem frozen cerebellar cortex of 15 patients with ET and 15 controls (Student's t-test). (**B**) Correlation analysis of mGluR1 expression and the percentage of CF synapses on the thin, spiny PC dendritic branchlets (11 ET and 8 controls, Pearson's correlation) (**C**) Correlation analysis of mGluR1 expression and the percentage of CFs extending to the outer 20% of the molecular layer (11 ET and 8 controls, Pearson's correlation).

Supplementary Figure 2

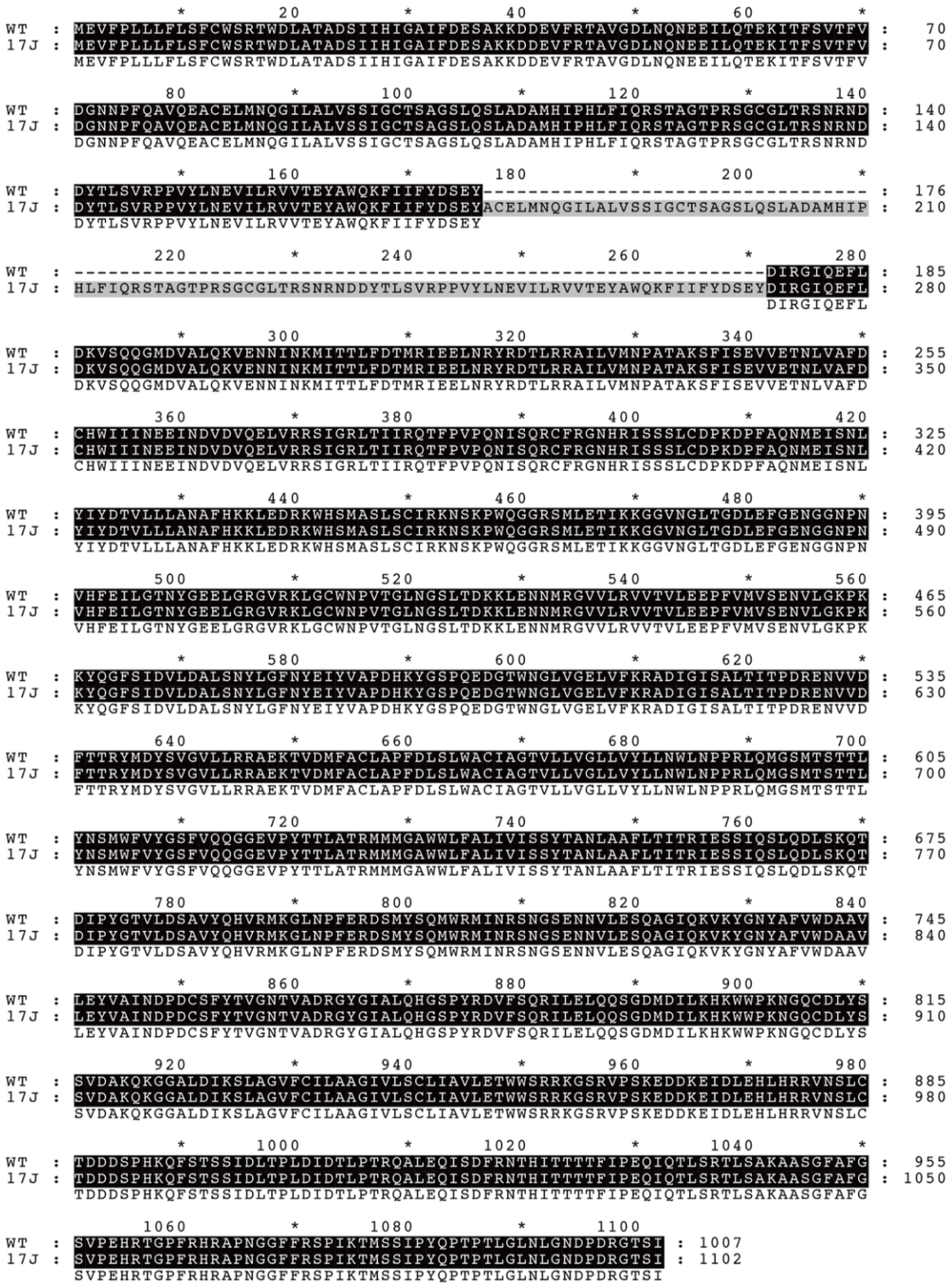

Fig. S2. The amino acid alignment of the protein products of WT and *hotfoot17J* GluRδ2 cDNA.

Supplementary Figure 3

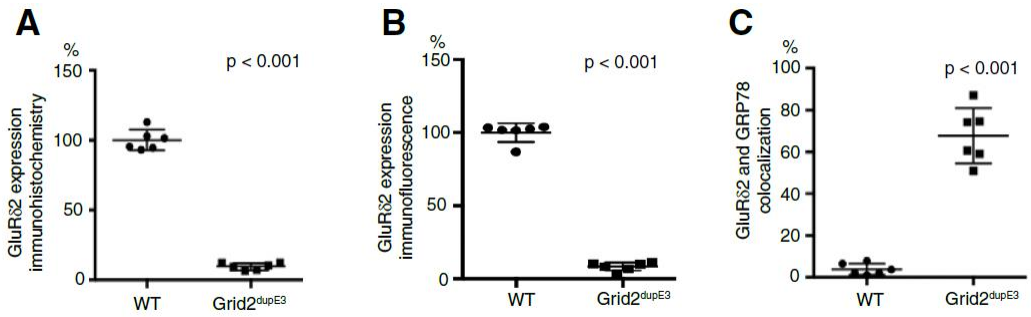

Fig. S3. Quantification of cellular and subcellular expression of GluRδ2 in WT and *Grid2*^{dupE3} cerebellum. (A) GluRδ2 expression in the WT and *Grid2*^{dupE3} mouse cerebellar cortex by immunohistochemistry (n = 6, Student's t-test). **(B)** GluRδ2 expression in the WT and *Grid2*^{dupE3} mouse cerebellar cortex by immunofluorescence (n = 6, Student's t-test). **(C)** Colocalization of GluRδ2 and GRP78 in the WT and *Grid2*^{dupE3} mouse cerebellar cortex (n = 6, Student's t-test).

Supplementary Figure 4

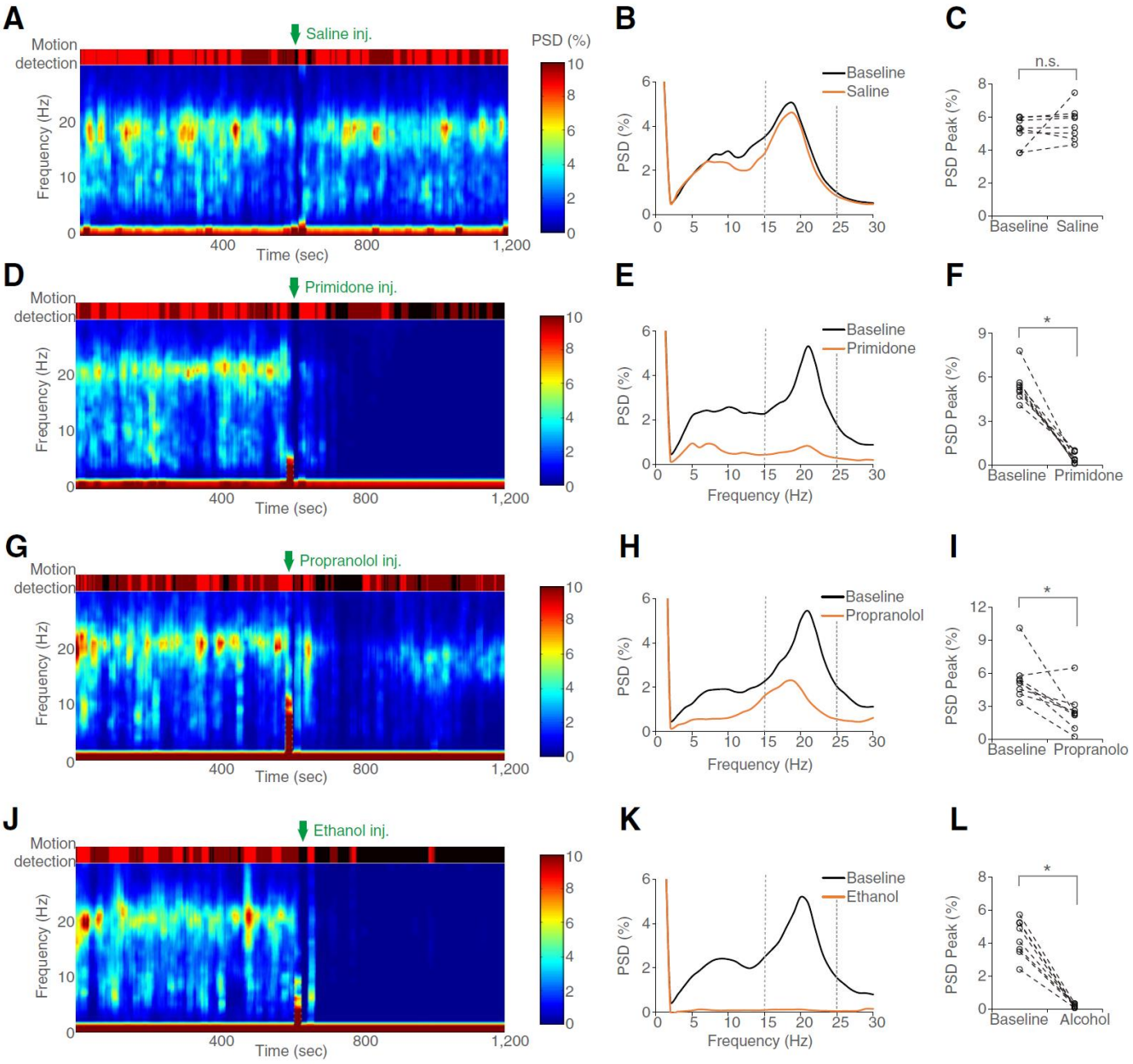

Fig. S4. Suppression of mouse tremor by ET medications. (A to **C)** Saline effect showed in representative time-frequency plot (A), corresponding spectral diagram (B) and group analysis (C). **(D** to **L)** Effects of primidone (D to F), propranolol (G to I) and ethanol (J to L). n = 8 mice at 4~6 months old for each agent. n.s.: not significant. * $p < 0.05$ by Wilcoxon Signed Ranks tests.

Supplementary Figure 5

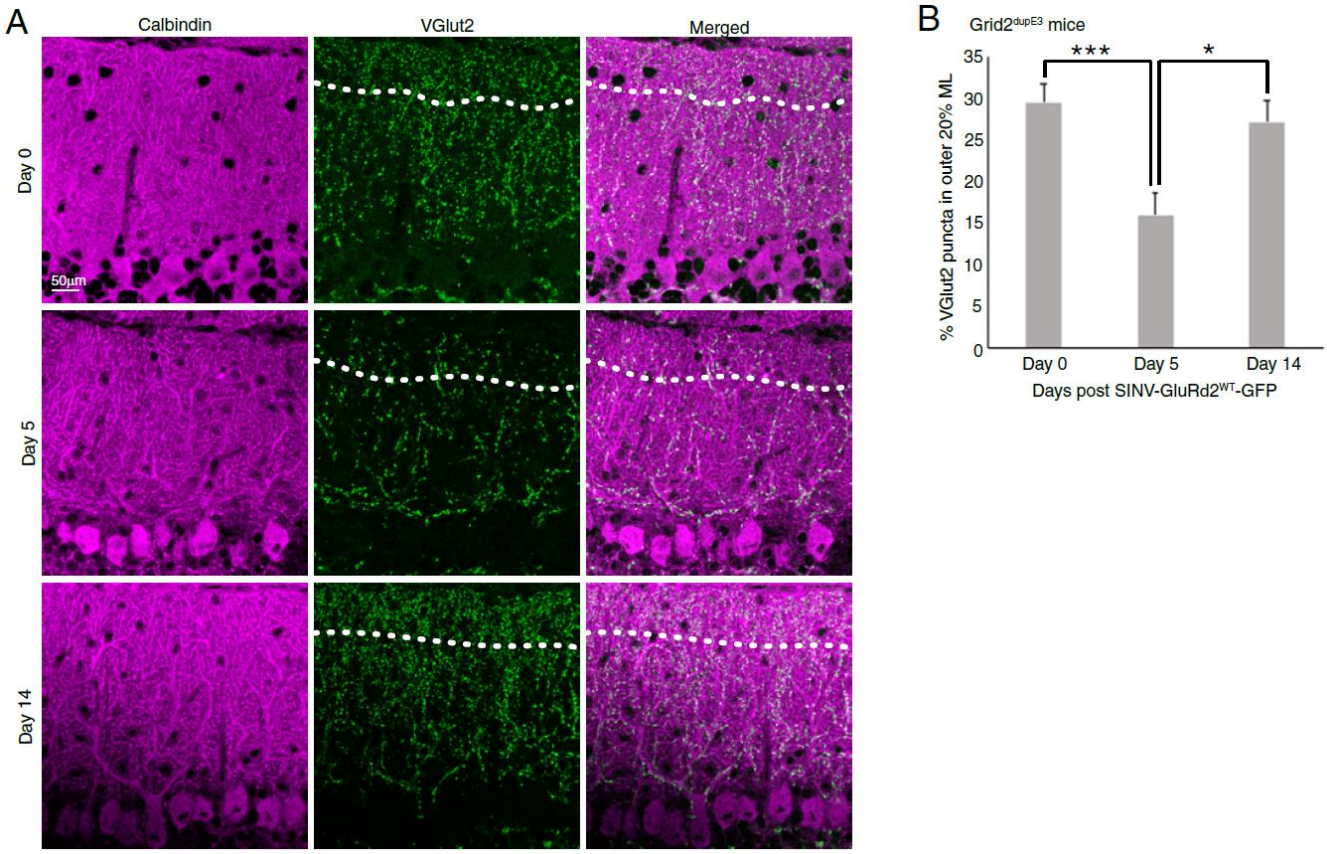

Fig. S5. Regression of CF synapses after rescue of GluRδ2 expression. (**A**) Representative images of CF synapses in the cerebellar cortex of *Grid2*^{dupE3} mice before SINV- GluRδ2^{WT}-GFP injection in the cerebellum (Day 0) and at post-injection Day 5 and Day 14. (**B**) Quantification of percentage CF synapses in the outer 20% of the molecular layer in the cerebellar cortex of *Grid2*^{dupE3} mice transfected with SINV-GluRδ2^{WT}-GFP at different time points (n = 3 sections, n = 3 mice in each group). *$p < 0.05$ ***$p < 0.005$ by ANOVA followed by Tukey's posthoc tests.

Supplemantary Figure 6

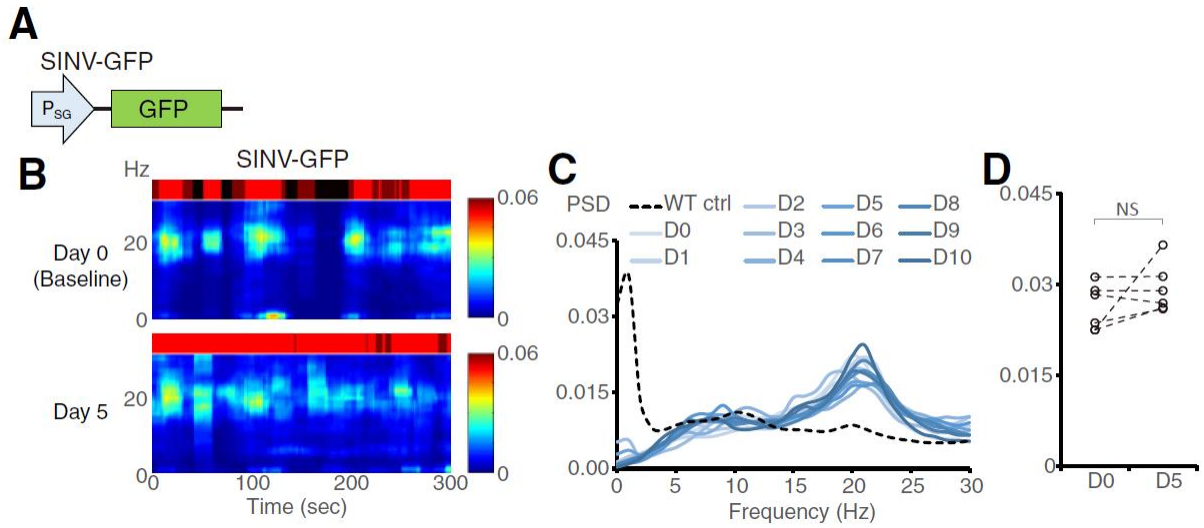

Fig. S6. Tremor in *Grid2*^{dupE3} mice receiving intracerebellar injection of control SINV. (**A**) The design of control Sindbis virus carrying GFP (SINV-GFP). **(B)** Representative time-frequency plots of tremor in a *Grid2*^{dupE3} mouse receiving SINV-GFP injection. **(C)** Serial PSD diagrams of tremor in a series of post-injection time points in the same mouse. Tremor modulatory effect was observed from day 0 (D0) to post-injection day 10 (D10) (**D**) Group analysis of tremor modulatory effect by SINV-GFP (*n* = 6 mice, NS: not significant by Wilcoxon Signed Ranks test).

Supplementary Figure 7

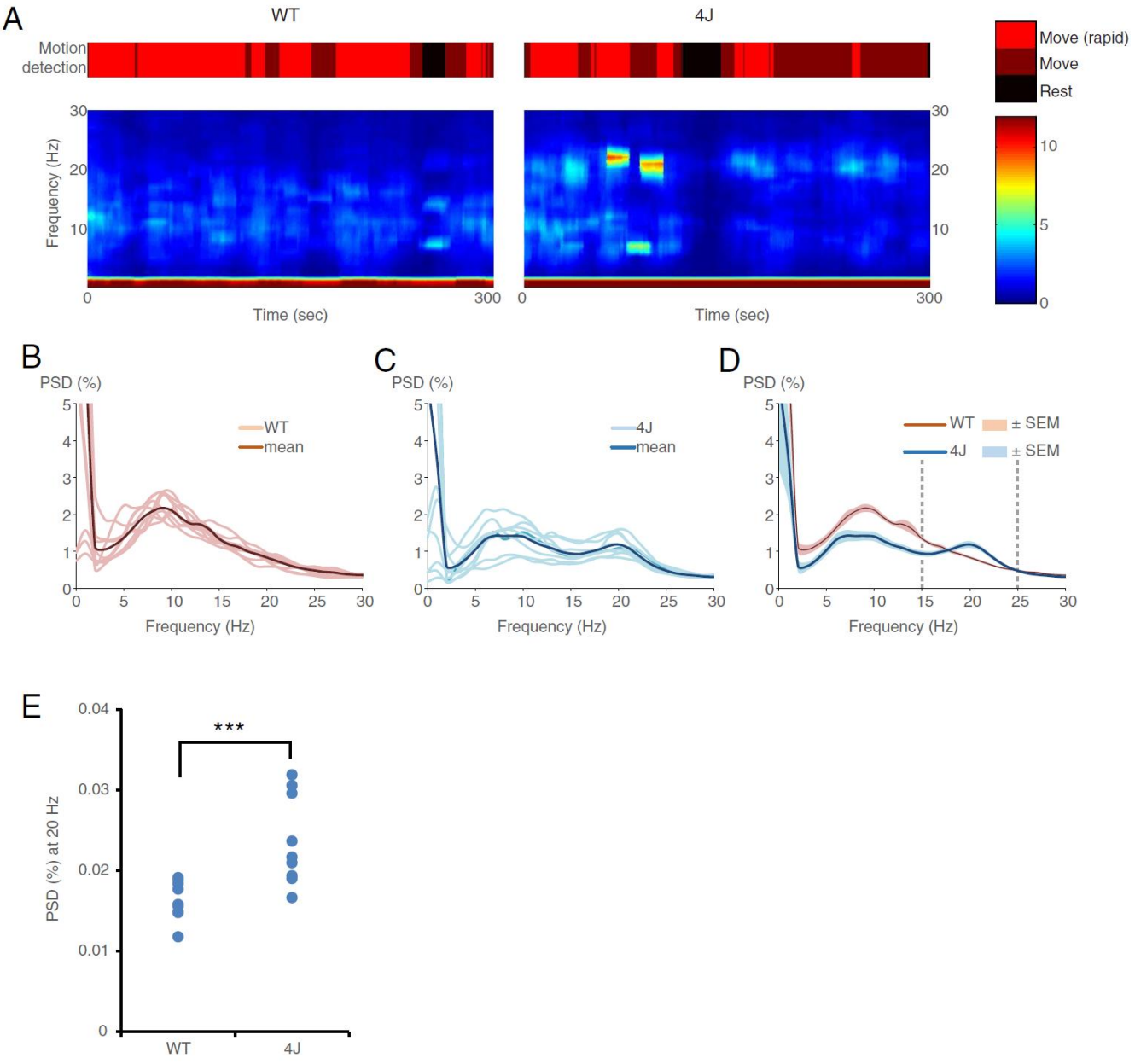

Fig. S7. Tremor in *hotfoot4J* mice. (A) Representative time-frequency plots of tremor in WT and *hotfoot4J* mice. **(B** to **E)** Group data of tremor PSD diagrams (n = 10 and 9 mice in WT littermates and *hotfoot4J* groups, respectively) and PSD statistics at 20 Hz. *** $p < 0.001$ by Mann-Whitney test.

Supplementary Figure 8

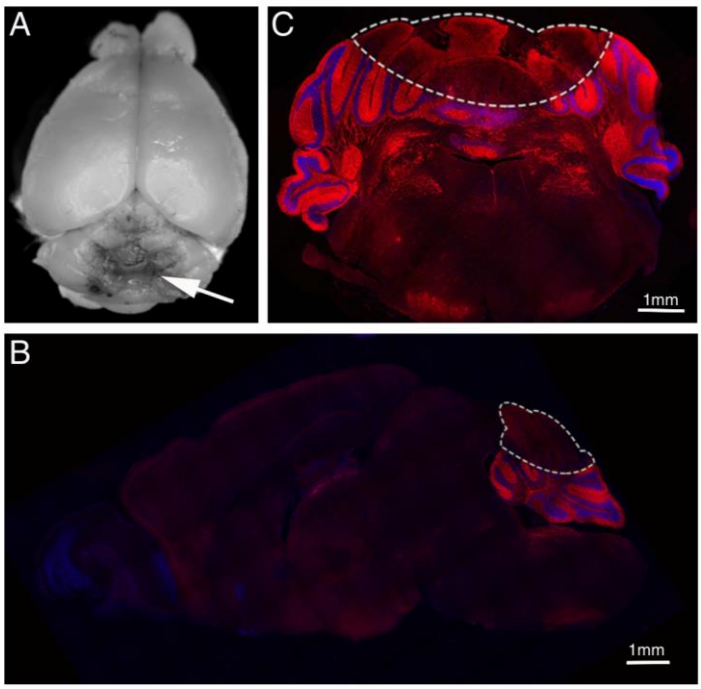

Fig. S8. Cryoinjury of mouse cerebellum by dry ice. (**A**) Whole brain view of the cerebellar damages after applying dry ice for 30 seconds. (**B** and **C**) Images of immunofluorescence labeled with calbindin (red) and DAPI (blue). Dry ice created damage within cerebellar cortex (C) and mainly in the motor cerebellum (B and C). **Fig. 4C** is the magnified photo of (B).

Supplementary Figure 9

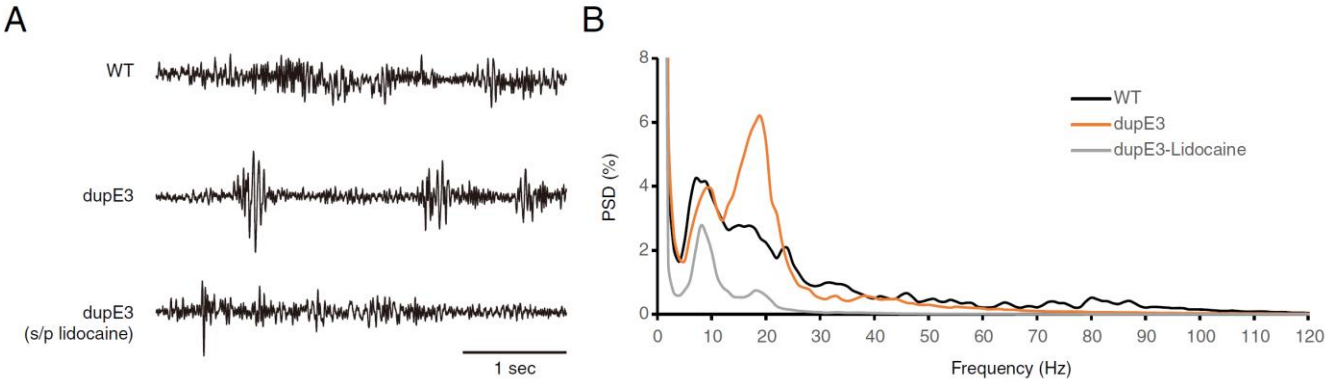

Fig. S9. Frequency profiles of tremor in *Grid2*^{dupE3} mice by IO silencing. (**A**) Raw sweeps of behavioral oscillations recorded by accelerometer in a WT mouse, a *Grid2*^{dupE3} mouse and a *Grid2*^{dupE3} mouse underwent intra-IO lidocaine micro-infusion. **(B)** PSD diagram. *Grid2*^{dupE3} mouse with lidocaine infusion in IOs did not develop tremor in other frequencies below 120 Hz.

Supplementary Figure 10

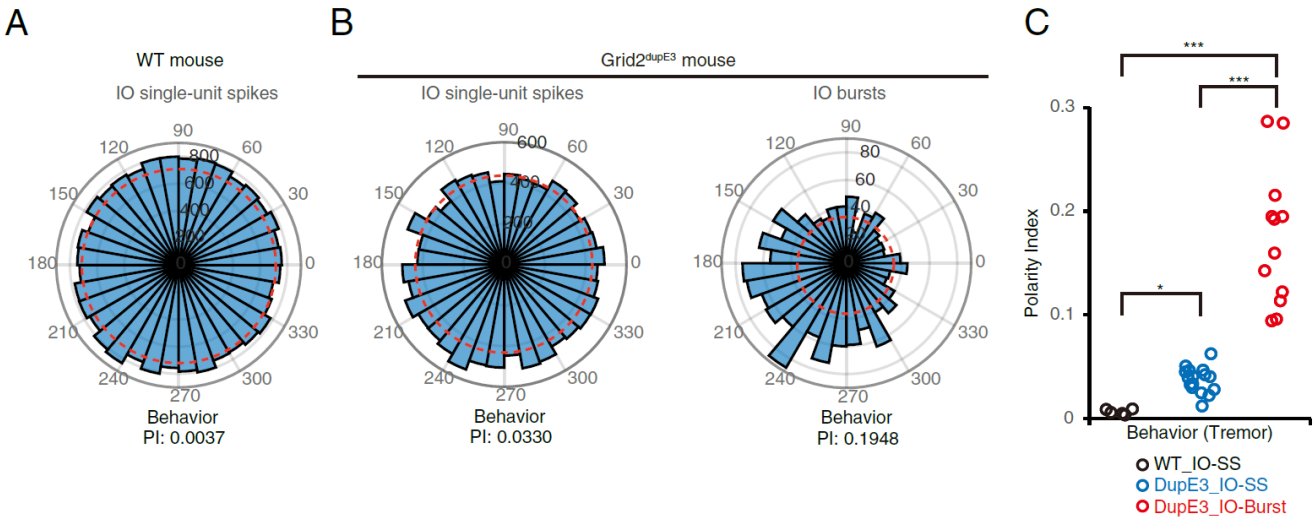

Fig. S10. Spike-phase coupling between IO spikes and tremor phases. Spike-phase coupling were calculated between IO spikes and Tremor. **(A** and **B)** Representative figures of angular histograms and corresponding polarity index (PI, see method) in a WT mouse (A), and a *Grid2*^{dupE3} mouse (B). **(C)** Group analysis of polarity index (n = 5, 16, 12 in WT_IO single-unit spike (WT_IO-SS), DupE3_IO-SS and DupE3_IO-burst groups, respectively). * $p < 0.05$; *** $p < 0.001$ by non-parametric Kruskal-Wallis test.

Supplementary Figure 11

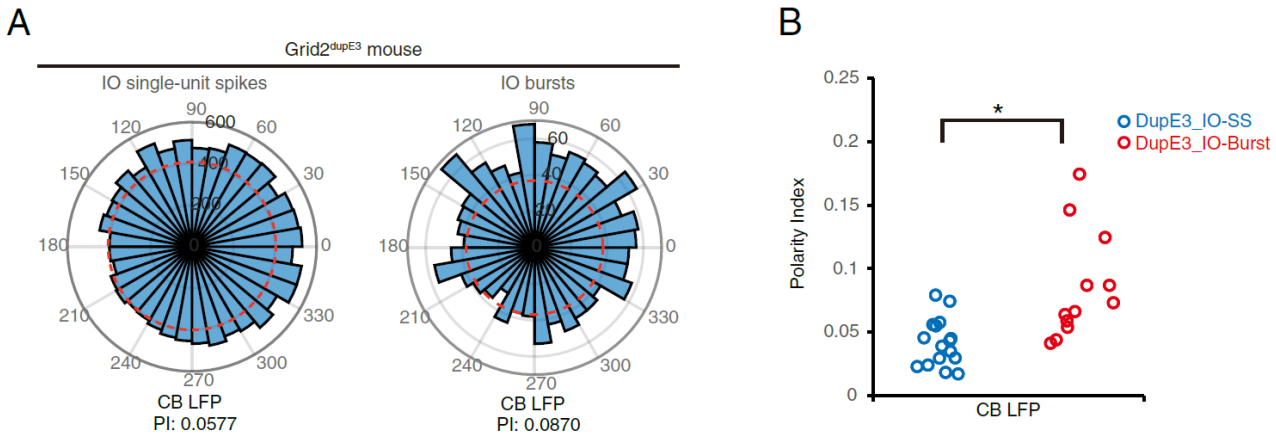

Fig. S11. Spike-phase coupling between IO spikes and cerebellar LFPs. Spike-phase coupling were calculated between IO spikes and cerebellar LFPs. **(A)** Representative figures of angular histograms and corresponding polarity index in a *Grid2*^{dupE3} mouse between single-unit spikes or burst activities in IO. **(B)** Group analysis of polarity index in *Grid2*^{dupE3} mice, calculated based on single-unit spikes or bursting spikes in IO (n = 16, 12 in DupE3_IO-SS and DupE3_IO-burst groups, respectively). * $p < 0.05$ by non-parametric Kruskal-Wallis test.

Supplementary Figure 12

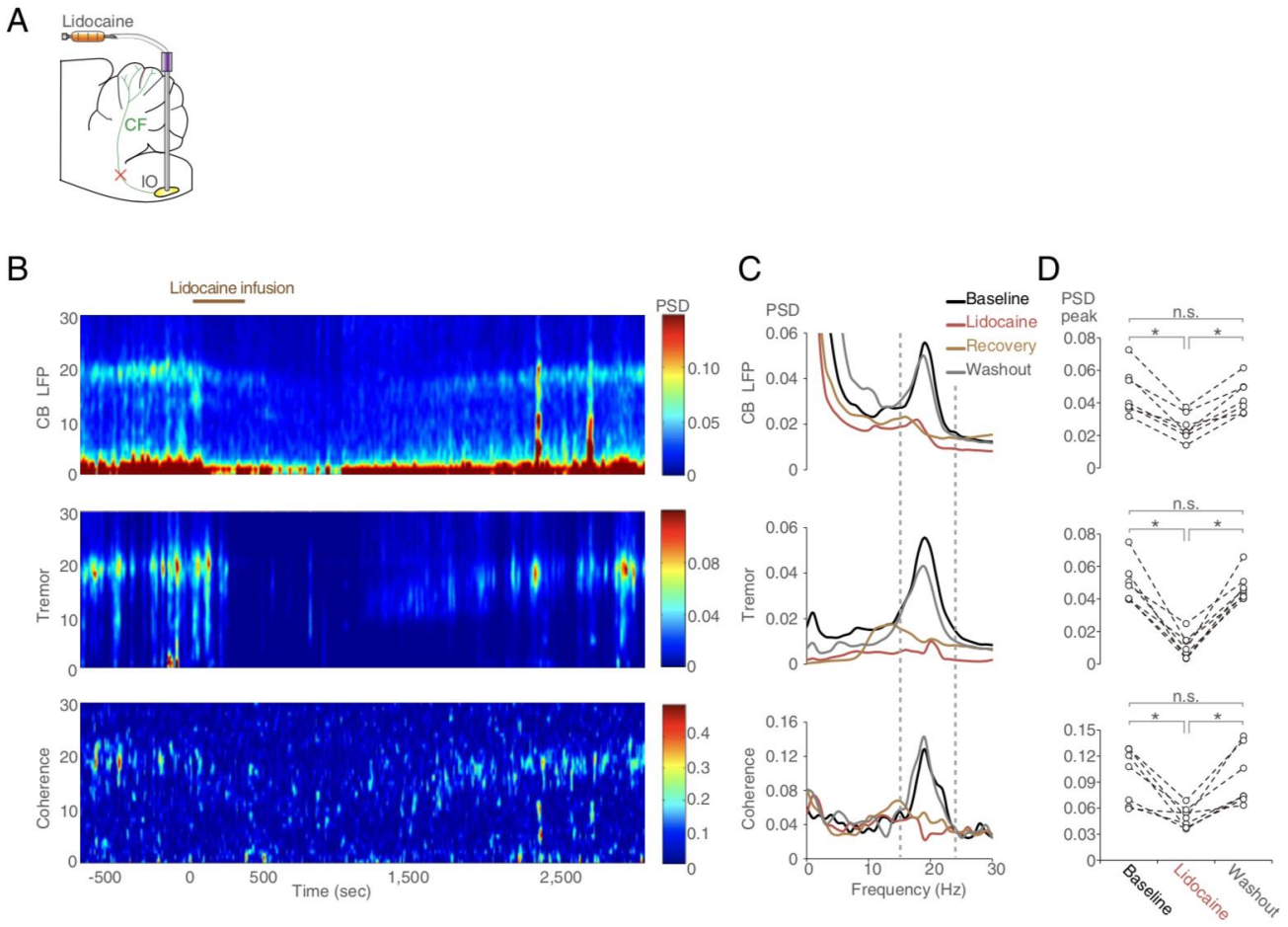

Fig. S12. Suppression of cerebellar oscillations and tremor by IO silencing.

(**A**) Experimental scheme. (**B** and **C**) Representative time-frequency plots (B) and PSD diagrams (C) of cerebellar oscillations, tremor, and their coherence in *Grid2*^{dupE3} mice. The tremor frequency spectrum is the same representative data showed in **Fig. 4M.** (**D**) Quantitative group analysis (n = 7 mice). *p < 0.05 by Wilcoxon Signed Rank tests. Error bars denote s.e.m. IO: inferior olive.

Supplementary Figure 13

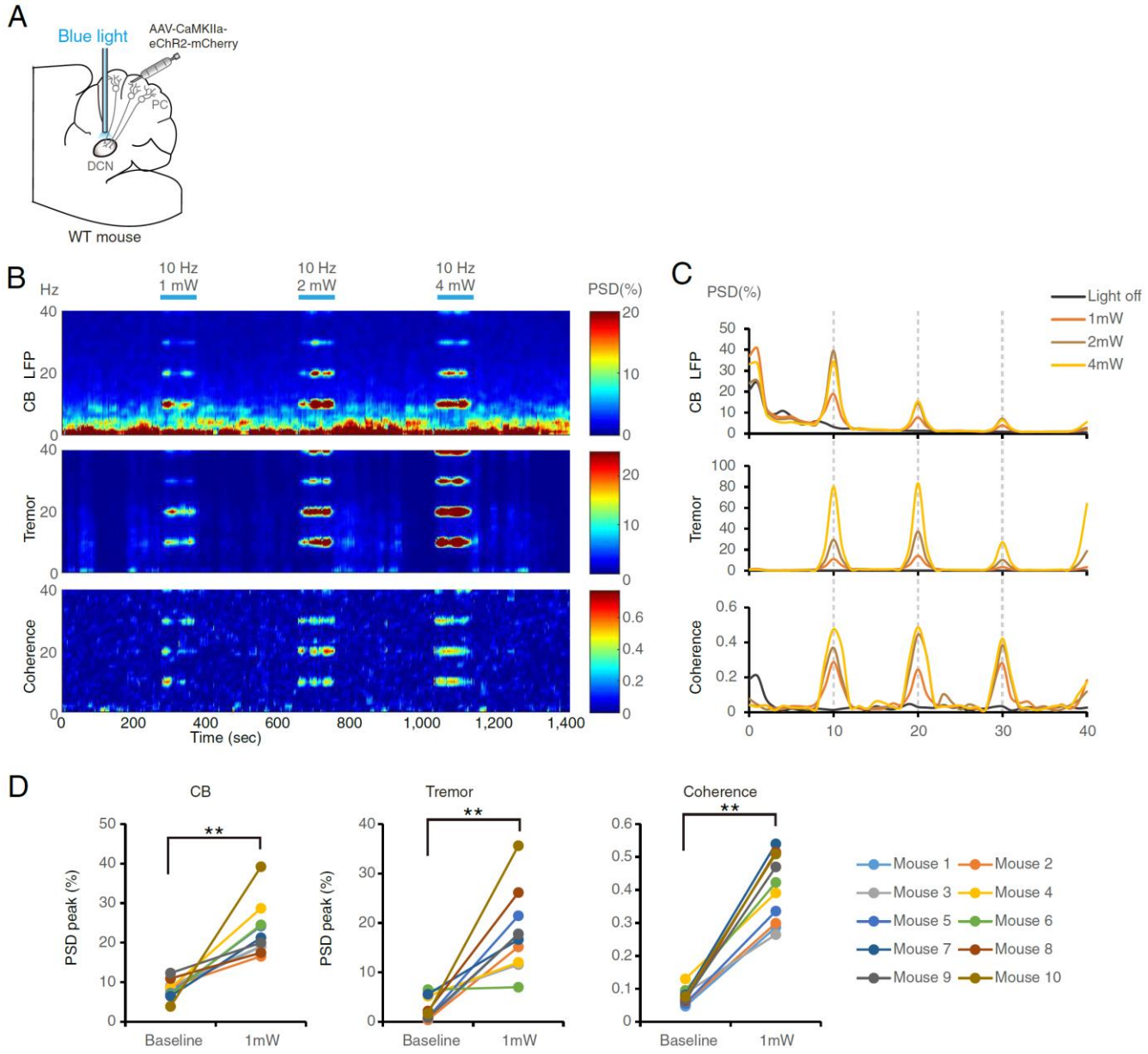

Fig. S13. Optogenetic stimulation of PC outputs at 10 Hz. (A) An experimental procedure similar to **Fig. 6E**, except that the optic simulation is given at 10 Hz. **(B** and **C)** Representative time-frequency plots (B) and PSD diagrams (C) showing oscillations at 10 Hz and its harmonic frequencies in both cerebellar LFPs and tremor. **(D)** Group analysis of 10-Hz optic stimulation (n = 10 mice). ** $p < 0.01$ by Wilcoxon Signed Ranks tests.

Supplementary Figure 14

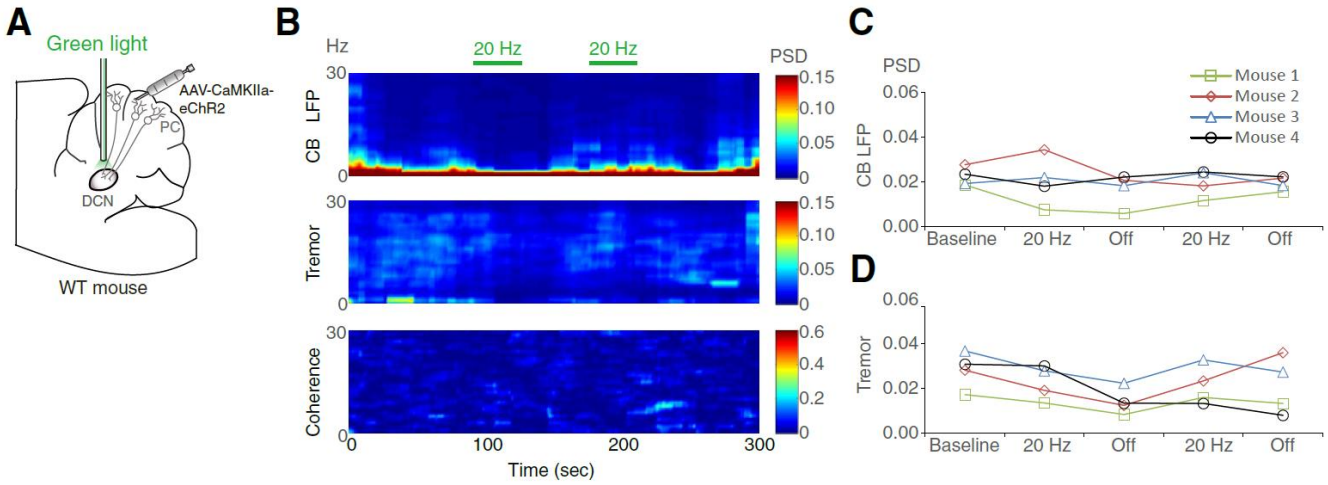

Fig. S14. Optogenetic stimulation of PC outputs by nonactivating green light. (A) A scheme showing eChR2 transfection in PCs and green light illumination in PC axonal terminals. The experimental design was the same as **Fig. 6E,** except for the green light (561 nm). **(B)** Representative time-frequency plots of cerebellar LFPs, tremor behaviors and their coherence. **(C** and **D)** Quantification of light effect on PSD peaks of cerebellar LFP (C) and tremor (D).

Supplementary Figure 15

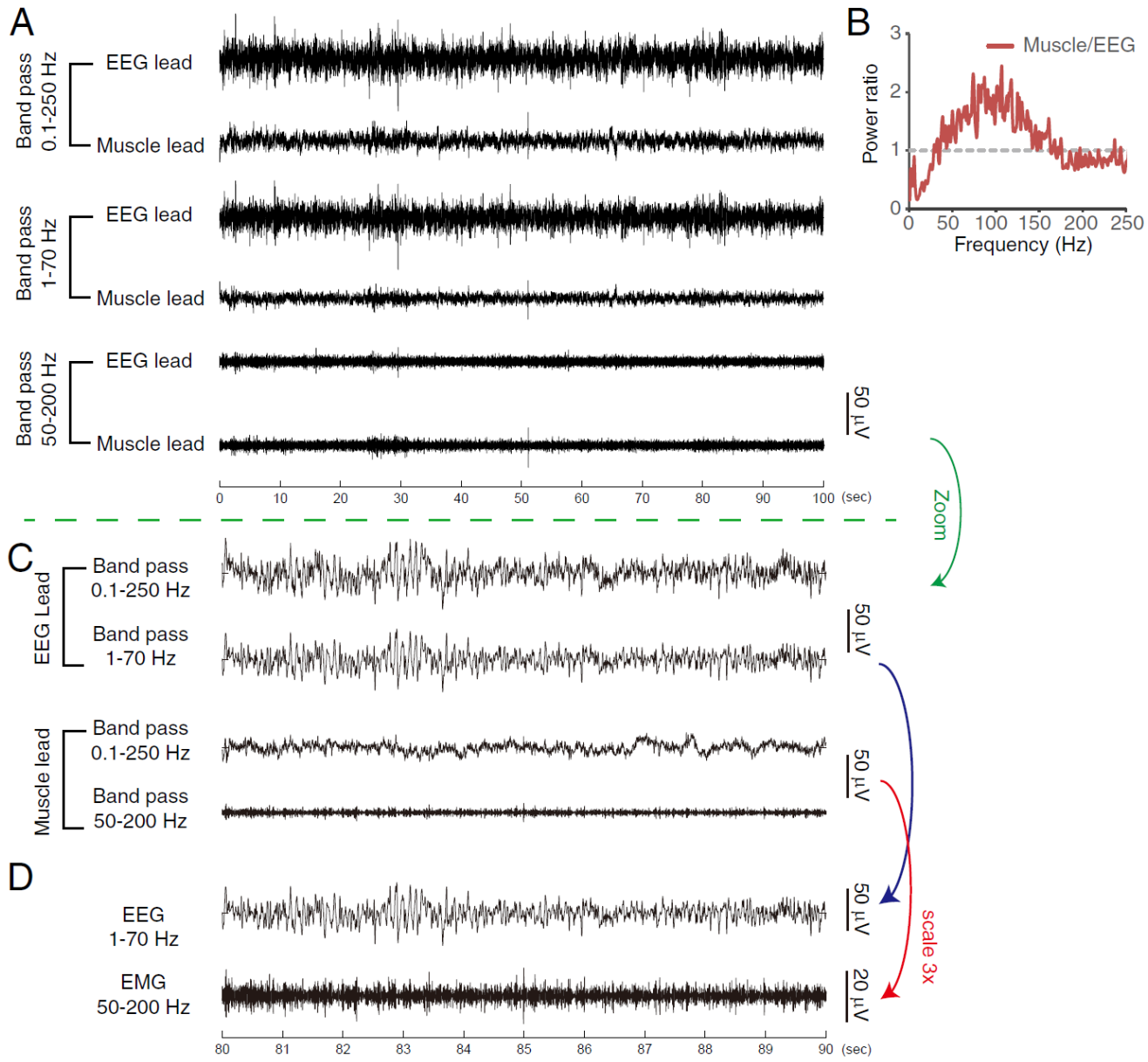

Fig. S15. Signals and characteristics of cerebellar EEG leads and nearby muscle leads. (A) Representative sweeps in raw recorded data (band-passed filter: 0.1-250 Hz), common filter settings for EEG (filtered between 1-70 Hz) and electromyography (EMG, filtered between 50-200 Hz). **(B)** Power ratios of muscle to EEG across recorded frequencies. **(C)** Magnified signals in typical EEG and EMG settings. EMG: electromyography.

Supplementary Figure 16

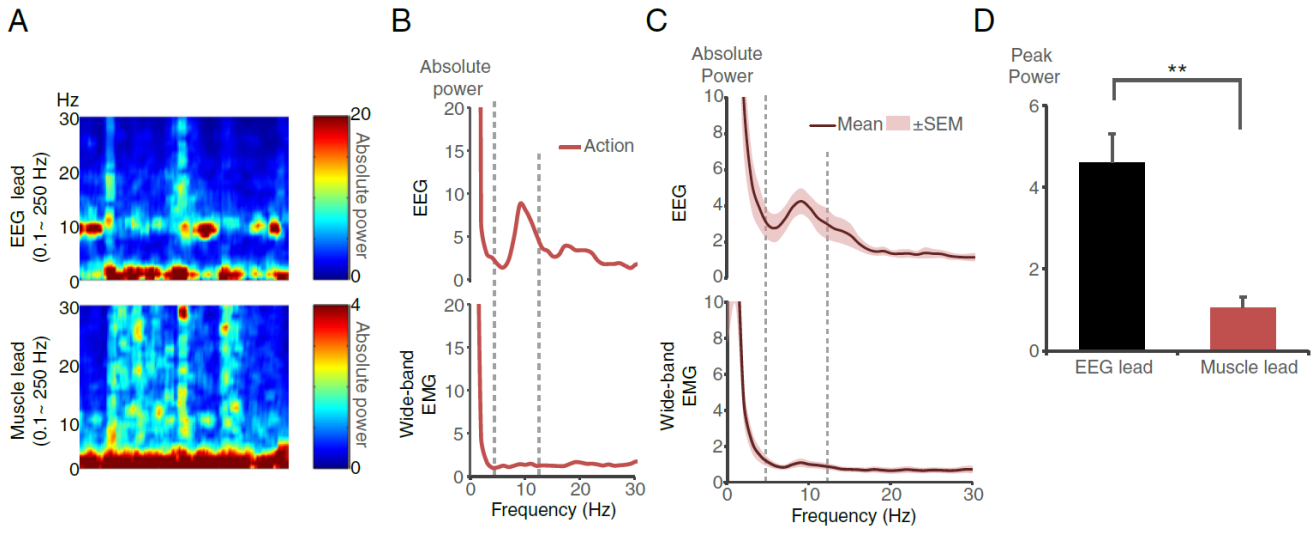

Fig. S16. Signal comparison between cerebellar EEG leads and nearby muscle leads in patients with ET. (A and **B)** Representative time-frequency plots and corresponding PSD diagrams in EEG and muscle leads. **(C** and **D)** Group analysis of PSD patterns (C) and quantification of PSD peaks (D). Spectral power in the tremor frequencies (4-12 Hz, dash lines) are ~5 times smaller in muscle leads (n = 10 patients). **$p < 0.01$ by Wilcoxon Sign Rank test. Error bars denote s.e.m.

Supplementary Figure 17

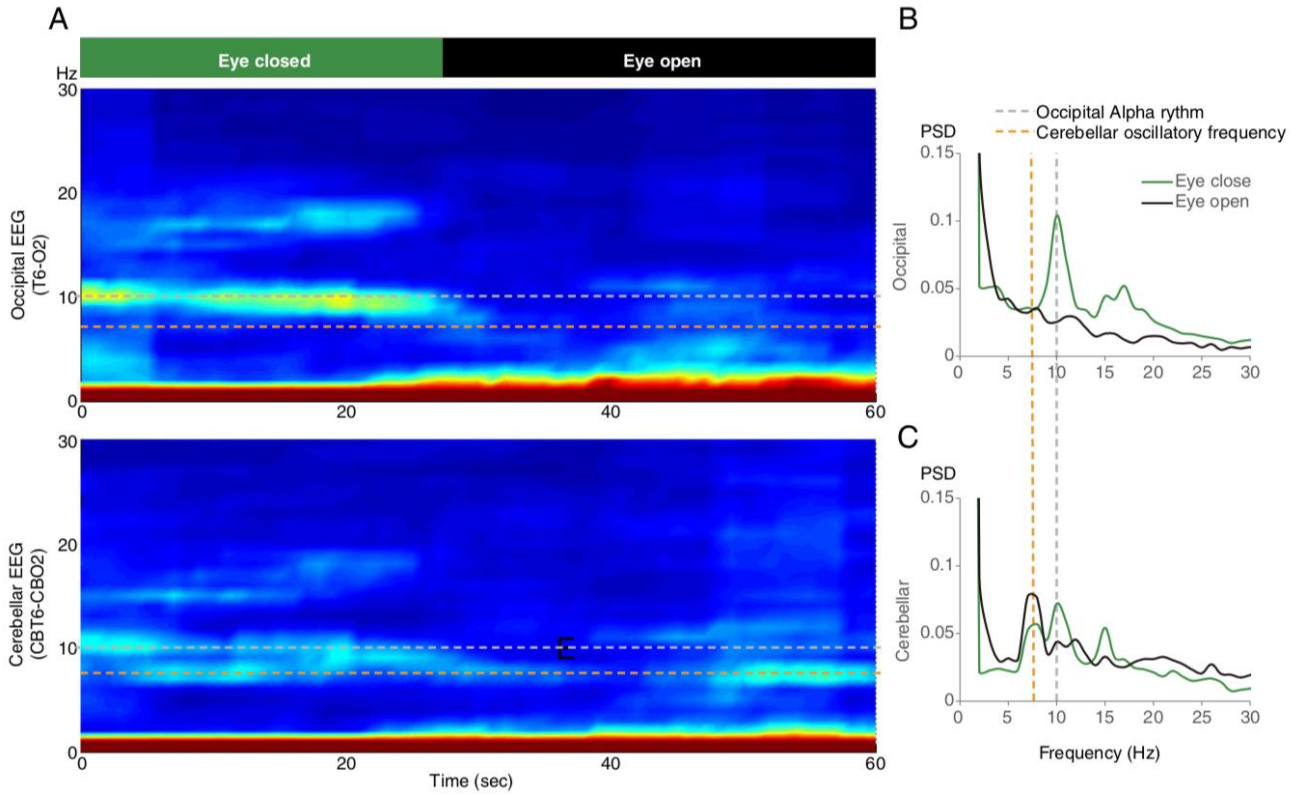

Fig. S17. Occipital alpha rhythm and cerebellar oscillations in a patient with ET. (A) Representative time-frequency plots in occipital leads (*top*) and cerebellar leads (*bottom*) during eye-closed and eye-open conditions. **(B)** Corresponding PSD diagrams. Cerebellar EEG showed a regional peak at 7 Hz during an eye-open condition, and there was no peak in the occipital area. Eye closing led to remarkable alpha rhythms in the occipital region at 10 Hz, which was also seen in cerebellar leads with lower amplitudes. The 7 Hz peak in the cerebellar region remained during eye closing. 7 Hz cerebellar oscillations are not modulated by eye opening or closing and are not the volume conduction from occipital alpha rhythm.

Supplementary Figure 18

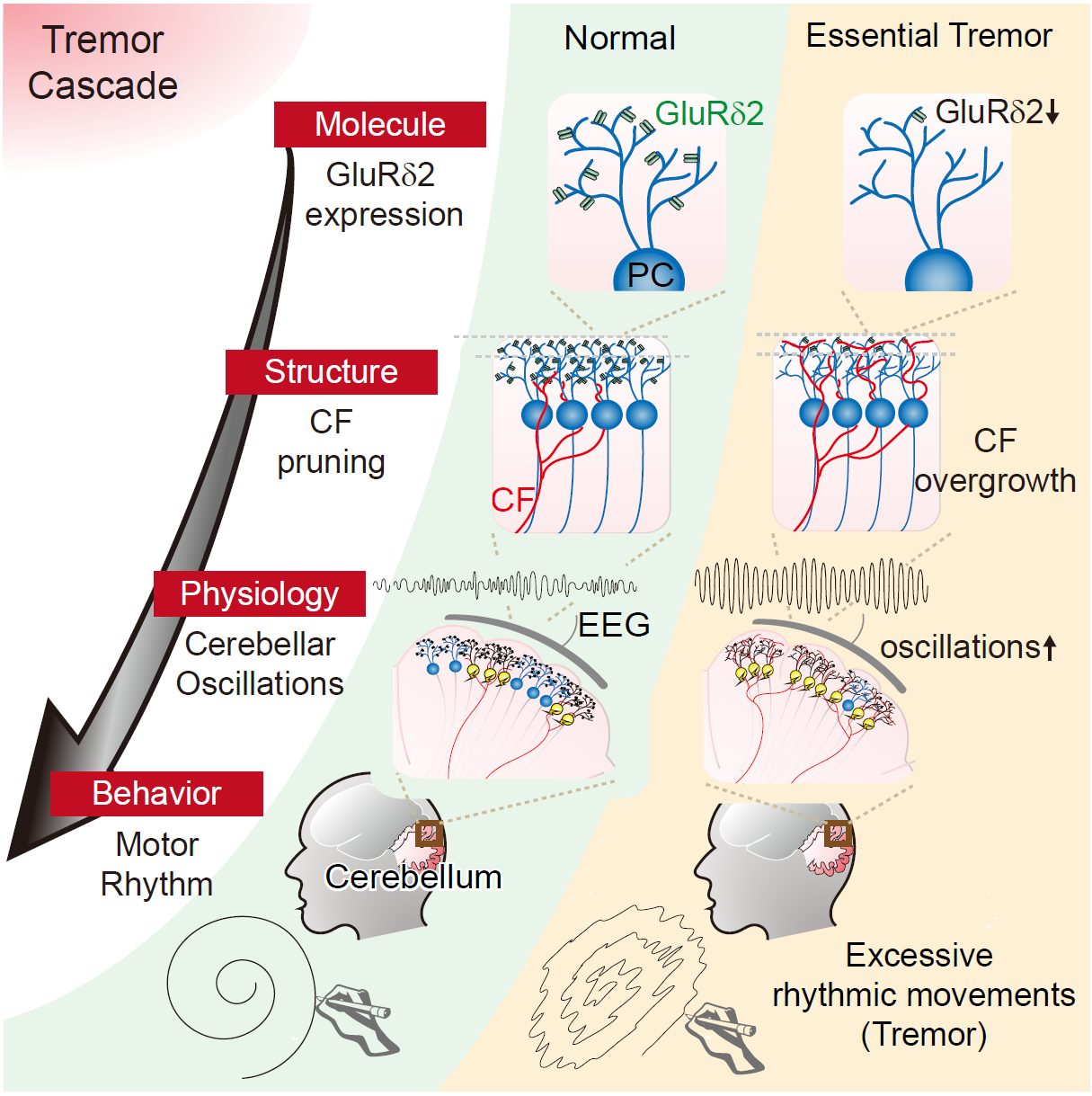

Fig. S18. CF synaptic pruning deficits, cerebellar oscillations, and tremor.
Patients with ET and *Grid2*^{dupE3} mice as two parallel systems in humans and mouse models that can be mutually referenced at the molecular, structural, physiological, and behavioral levels to understand the rhythm control of movements. GluRδ2 deficiency causes CF overgrowth and hyper-innervations on PCs, leading to excessive cerebellar oscillations that result in abnormal rhythmic movements, known as tremor.

SUPPLEMENTARY TABLES

Table S1. Clinical and pathological features of postmortem cerebellum in patients with ET and control subjects.

	Western blot analysis			Immunohistochemistry		
	ET	Controls	*p*	ET	Controls	*p*
n	15	15		15	19	
Age at death (years)	83.5 ± 56.2	80.3 ± 7.7	0.22*	82.6 ± 6.3	80.9 ± 6.3	0.46*
Female gender	7 (46.7%)	6 (40.0%)	0.72[#]	11 (73.3%)	11 (57.9%)	0.36[#]
Age of tremor onset	47.9 ± 19.5	NA		38.1 ± 23.7	NA	
Disease duration	34.6 ± 18.1	NA		44.4 ± 22.8	NA	
Total tremor scores	24.5 ± 5.1	NA		24.6 ± 4.9	NA	
Presence of head tremor	5 (33.3%)	NA		8 (53.3%)	NA	
Presence of voice tremor	4 (26.7%)	NA		4 (26.7%)	NA	
Family history of tremor	3 (20.0%)	NA		6 (40.0%)	NA	
Purkinje cell counts	9.1 ± 1.4	11.2 ± 1.2	**0.00***	8.9 ± 0.9	11.4 ± 1.2	**0.00***
Purkinje cell axonal torpedoes	14.1 ± 12.1	4.2 ± 4.7	**0.01[&]**	19.3 ± 21.8	4.3 ± 4.3	**0.02[&]**

Data are presented with Mean ± Standard deviation

ET = essential tremor, NA = not applicable

*Student t-test

[#]chi-square analysis

[&]Mann-Whitney analysis

Table S2. Demographic data of patients with ET and control subjects for the EEG study.

	Essential tremor	Control
n	10	10
Age (years)	62.2 ± 14.9	59.4 ± 16.6
Female gender	3 (30%)	3 (30%)
Age of tremor onset	39.9 ± 22.8	NA
Disease duration	22.3 ± 12.8	NA
Total tremor scores	16.7 ± 8.1	NA
Presence of head tremor	5 (50%)	NA
Presence of voice tremor	2 (20%)	NA
Family history of tremor	7 (70%)	NA
ET Medication use	5 (50%)	NA
β-blocker	3 (30%)	NA
primidone	2 (20%)	NA
topiramate	1 (10%)	NA

ET: essential tremor, NA: not applicable

Table S3. Demographic data of patients with ET and control subjects for cerebellar oscillation index.

	Essential tremor	Control	P value
n	20	20	
Age (years)	59.9 ± 9.8	57.9 ± 16.3	0.642[a]
Female gender	9 (45%)	10 (50%)	0.752[b]
Age of tremor onset	37.2 ± 17.3	NA	
Disease duration	23.2 ± 9.1	NA	
Total tremor scores	21.5 ± 9.1	0.2 ± 0.3	**<0.001**[a]
Family history of tremor	15 (75%)	0	**<0.001**[a]
COI	11.6 ± 4.9	8.3 ± 4.4	**0.031**[a]

NA, not applicable; COI: cerebellar oscillatory index

[a]independent t-test

[b]ch-square analysis

Movie S1. Tremor characteristics in WT versus *Grid2*^{dupE3} mice.

As compared to normal mice, *Grid2*^{dupE3} mice showed marked tremor in limbs, head, and trunk. The tremor was action-dependent and not observed at rest.

Movie S2. Tremor modulation by dry ice–mediated cerebellar lesioning.

Cerebellar lesioning by dry ice significantly suppressed tremor

Movie S3. Tremor modulation by optogenetic inhibition of cerebellar outputs.

Comparing to the baseline tremor, optogenetically inhibition of PC axonal terminals at DCN suppressed limb tremor. Immediate suppression of head tremor was also observed after illumination.

Movie S4. Tremor modulation by synaptic inhibition of CFs.

This *Grid2*^{dupE3} mouse received blue-light scanning of the cerebellar surface via a transparent cranial window. Tremor was significantly suppressed afterward and returned to baseline after 24 hours.

Movie S5. Tremor induction by PC stimulation in a WT mouse.

Optogenetic activation of PC axonal terminals at 20 Hz generated immediate body and limb tremor in a WT mouse.

Data file S1. Raw data (provided as separate excel file).